The Journal of Green Energy and Environmental Engineering

Research Paper

Application of Polyethylenimine Modified Nickel Ferrite Graphene Oxide Composite in the Enrichment of Phosphopeptides

Victoria Li[1], Daniel Park[1], Imteaz Mondol[2,*]

[1] IMT Atlantique, LS2N - CNRS, La Chantrerie, 4 rue Alfred Kastler, 44307 Nantes, France
[2] Department of Chemistry and Green-Nano Materials Research Center, Kyungpook National University, Daegu 41566, South Korea
*Corresponding author: Victoria@imt-atlantique.fr; Parkbuss06@imt-atlantique.fr; Mondol@knu.ac.kr

Abstract. A polyethyleneimine (PEI)-modified nickel ferrite-graphene oxide composite material, GO@PEI-$NiFe_2O_4$, was prepared for the selective purification and enrichment of phosphopeptides from biological samples. The Ni^{2+} and Fe^{3+} ions on its surface can coordinate with phosphate groups, thereby selectively adsorbing phosphopeptides. The modified PEI enhances the hydrophilicity of the composite, which facilitates its binding to phosphopeptides. In addition, $NiFe_2O_4$ in the composite is magnetic, enabling its rapid separation from solution. Using β-casein as a sample, the enrichment performance of the composite for phosphopeptides in tryptic digest was investigated, and the results were compared with those enriched by GO@$NiFe_2O_4$ (without PEI modification). The adsorption mechanism of the composite was also discussed. The static and dynamic adsorption curves of the composite for pTyr were determined using the phosphopeptide pTyr, and the maximum adsorption capacity reached 36.2 μg/mg. The results showed that this composite could effectively remove the interference of non-phosphopeptides and efficiently enrich phosphopeptides in complex matrices. After enrichment of tryptic digest of rat liver proteins, 1535 phosphopeptides were identified by mass spectrometry, and the enrichment effect was significantly better than that of a commercial Fe^{3+}-IMAC kit. This study provides a highly selective material for the enrichment of phosphopeptides and shows potential application in phosphoproteomics research.

Keywords: *phosphopeptides; nickel ferrite; polyethyleneimine; graphene oxide; magnetic responsen*

Received on 02 March 2026, Accepted on 05 June 2026, Published on 07 July 2026

1 Introduction

Many important physiological and biochemical activities in organisms are related to protein phosphorylation, such as cell signal transduction, differentiation, and proliferation [1-3]. Abnormal protein phosphorylation can also lead to the occurrence and development of many diseases [4-8]. Studying protein phosphorylation helps to reveal the mechanisms of disease occurrence and development and discover related disease biomarkers, thus attracting much attention. Mass spectrometry (MS) has become an indispensable analytical tool in proteomics research due to its strong qualitative and quantitative analysis capabilities, fast analysis speed, high throughput, high resolution, and high sensitivity [9-11]. However, the identification of phosphorylated proteins in complex biological samples cannot be directly detected by MS due to large sample matrix interference and low abundance of the target components [12-13]. Before mass spectrometry analysis of phosphopeptides, samples usually need to be purified and enriched first to remove the influence of interfering components [14]. Therefore, the performance of enrichment materials plays a key role in the identification of phosphorylated proteins. The development of efficient and highly specific enrichment materials is crucial for the detection of phosphorylated proteins.

Metal oxide affinity chromatography (MOAC) has a good enrichment effect on phosphopeptides in complex matrices. The metal cations on the surface of the enrichment material can specifically recognize the phosphate

groups of phosphopeptides and form complexes [15-16]. These metal cations are bonded to oxygen atoms through chemical bonds, with strong stability and are not easily lost during the enrichment process. Various MOAC metal oxides for phosphopeptide enrichment have been reported [17-22], such as TiO_2, CeO_2, and MoO_3. These metal oxides have good selectivity for enriching phosphopeptides in complex matrices. However, most metal oxides have low hydrophilicity, which limits their purification and enrichment effects on phosphopeptides to some extent. Therefore, modification of metal oxides has become a research hotspot in recent years [23-24].

Nickel ferrite is a binary metal oxide. The Ni-O and Fe-O functional group clusters contained in its molecules can selectively bind to phosphopeptides [25-26], so it can be used as an enrichment material for phosphopeptides in biological samples. At the same time, $NiFe_2O_4$ molecules contain ferrite, which is a magnetic substance and can be rapidly separated from solution in the presence of a magnet [27]. However, without modification, $NiFe_2O_4$ as an enrichment material has poor adsorption performance for phosphopeptides [25-26] and is highly prone to aggregation, making it inconvenient to use and affecting the enrichment effect [28].

In this study, a solvothermal method was used to simultaneously modify $NiFe_2O_4$ and polyethyleneimine (PEI) on the surface of graphene oxide (GO) to prepare a GO@PEI-$NiFe_2O_4$ magnetic composite material. PEI, as a water-soluble polymer, can improve the hydrophilicity of the enrichment material. The introduction of GO reduces the aggregation of magnetic materials and increases their dispersibility in polar solvents. The results show that the GO@PEI-$NiFe_2O_4$ magnetic composite can highly selectively enrich phosphopeptides in complex biological samples. The enrichment effect is significantly better than that of commercial Fe^{3+}-IMAC kits, and it can complement TiO_2 enrichment materials, showing good application potential in phosphoproteomics research.

2 Experimental Section

2.1 Instruments and reagents

Nicolet iS50 infrared spectrometer (FTIR, Thermo Scientific, USA); JEM-2100F field emission transmission electron microscope (TEM) and attached energy-dispersive X-ray spectrometer (EDX, JEOL, Japan); S-4800 scanning electron microscope (SEM, Hitachi, Japan); SmartLab X-ray diffractometer (XRD, Rigaku, Japan); SQUID-VSM magnetic measurement system (Quantum Design, USA); H-Class ultra-high performance liquid chromatograph (UPLC, Waters, USA); Autoflex Speed matrix-assisted laser desorption/ionization time-of-flight mass spectrometer (MALDI-TOF, Bruker, Germany); 1200-Orbitrap Lumos nano liquid chromatography-mass spectrometer (nano LC-MS, Thermo Scientific, USA).

Ferric chloride ($FeCl_3·6H_2O$, analytical grade), nickel nitrate ($Ni(NO_3)_2·6H_2O$, analytical grade), polyethyleneimine (PEI, molecular weight ~70 000), ethylene glycol, ammonia ($NH_3·H_2O$, 25%–28%), sodium acetate, trifluoroacetic acid (TFA, >99.5%), formic acid (FA) and ethanol (analytical grade) were purchased from Aladdin Company. Bovine β-casein (β-Casein, ≥98%), PHOS-Select™ iron affinity gel (Fe^{3+}-IMAC kit) and bovine serum albumin (BSA, ≥98%) were purchased from Sigma-Aldrich (Shanghai). Single-layer graphene oxide (GO, 98%) was from Siciou Technology Co., Ltd. Phosphopeptide pTyr (STSSDQPS[pY]SLE, molecular weight 1380.3, 98%) was from Qilio Biotechnology Co., Ltd. Desalting kit (Oasis HLB cartridges) was from Waters. Titansphere™ Phos-TiO_2 kit was from Shimadzu. Ultrapure water was prepared using a Milli-Q system (Millipore, USA). All chemical reagents were used directly without further purification.

2.2 Preparation of materials

GO@PEI-$NiFe_2O_4$ was prepared with improvements based on our previous work [29]. Briefly, 2.70 g $FeCl_3·6H_2O$ and 1.45 g $Ni(NO_3)_2·6H_2O$ were dissolved in 70 mL ethylene glycol under magnetic stirring. Then, 0.100 g PEI and 0.100 g GO were added and stirred until homogeneous. Under vigorous stirring, 10.8 g sodium acetate was added and stirring continued for 30 min. The mixture was transferred to a reactor and heated at 200 °C for 24 h. After cooling, the product was washed three times with pure water and anhydrous ethanol, respectively, and dried in a vacuum oven at 40 °C to obtain GO@PEI-$NiFe_2O_4$. For comparison, $NiFe_2O_4$ was prepared without adding GO and hydrophilic PEI; GO@$NiFe_2O_4$ was prepared without adding PEI, following the same procedure.

2.3 Enrichment of phosphopeptides by materials

Biological samples β-casein, BSA and rat liver proteins were all digested with trypsin, and the whole process referred to our previous work [29].

2.3.1 Enrichment of biological samples by GO@PEI-NiFe2O4 material

(1) Enrichment of tryptic digests of β-casein and β-casein/BSA: GO@PEI-$NiFe_2O_4$ was dispersed in 0.1% FA at a concentration of 10.0 mg/mL, mixed well. A 10.0 μL aliquot of the suspension was taken, washed twice with solvent A (50% ACN, 5% FA), magnetically separated, and the supernatant discarded. The sample to be enriched was dissolved in solvent A, and 50.0 μL was mixed with the GO@PEI-$NiFe_2O_4$ material, shaken at 600 r/min for 30 min, magnetically separated, and the supernatant discarded. The material was washed with 100 μL solvent A under shaking for 30 min, repeated three times. Phosphopeptides were eluted with 50.0 μL 10% $NH_3 \cdot H_2O$ for 30 min. The eluate was dried by vacuum concentrator and stored at −20 °C for subsequent analysis.

(2) Enrichment of rat liver digest: 2.00 mg GO@PEI-$NiFe_2O_4$ material was washed with solvent A. A 500 μg peptide sample was reconstituted in 300 μL solvent A, added to the enrichment material, and shaken for 30 min. After washing three times with 400 μL solvent A for 30 min each, phosphopeptides were eluted with 200 μL 10% $NH_3 \cdot H_2O$. The eluate was acidified with 120 μL 50% TFA, desalted, dried, and stored at −20 °C.

2.3.2 Enrichment process of phosphopeptides by TiO2

The material was balanced with solution B (80% ACN containing 0.4% TFA) and solution C (75% solution B containing 25% lactic acid), centrifuged, and the flow-through discarded. The peptide sample was dissolved in solution C, loaded onto the TiO_2 enrichment column, centrifuged, and the flow-through was reloaded onto the enrichment column and centrifuged again. Then, washed once with 20.0 μL solution C, and three times with solution B. Finally, eluted with 50.0 μL 5% $NH_3 \cdot H_2O$ and 50.0 μL 5% pyrrolidine, respectively, by centrifugation for 5 min. The eluates were combined, acidified with 100 μL 20% TFA, desalted, dried, and stored at −20 °C.

2.3.3 Enrichment process of Fe3+-IMAC kit (referring to its enrichment method)

The material was balanced three times with solution D (250 mmol/L acetic acid containing 30% ACN), each time vortexed to ensure full balance, and the solvent was removed by centrifugation. The peptide sample was reconstituted in solution D, added to the enrichment material, and incubated with vortexing. After centrifugation, the material was washed with solution D and water, then eluted with 400 mmol/L $NH_3 \cdot H_2O$. The eluate was acidified with 20% TFA, desalted, dried, and stored at −20 °C.

2.4 Determination of adsorption capacity and recovery

2.4.1 Static adsorption experiment

The adsorption capacity of GO@PEI-$NiFe_2O_4$ for phosphopeptides was evaluated using synthetic phosphopeptide pTyr. Seven portions of GO@PEI-$NiFe_2O_4$ material (35.0 μL, 10.0 mg/mL) were taken, washed with solvent A, then mixed with pTyr at masses of 5.00, 10.0, 20.0, 40.0, 80.0, 120 and 150 μg, respectively, and solvent A was added to a total volume of 100 μL. After shaking for 30 min, washed three times with 200 μL solvent A, and finally eluted with 100 μL 10% $NH_3 \cdot H_2O$. The eluate was acidified with 60.0 μL 50% TFA, centrifuged, and detected by high performance liquid chromatography (n=3).

2.4.2 Dynamic adsorption experiment

The experimental process was the same as static adsorption, except that the amount of pTyr was 80.0 μg, and the incubation time of GO@PEI-$NiFe_2O_4$ with pTyr was controlled at 1, 2, 5, 10, 20, 30 and 45 min, respectively.

3 Results and discussion

3.1 Preparation of GO@PEI-NiFe2O4 magnetic composite and its enrichment principle for phosphopeptides

Fig. 1A shows the preparation process of the magnetic composite GO@PEI-$NiFe_2O_4$. GO, PEI, $FeCl_3 \cdot 6H_2O$ and $Ni(NO_3)_2 \cdot 6H_2O$ were dispersed in ethylene glycol, heated in a reactor at 200 °C for 24 h, and the composite GO@PEI-$NiFe_2O_4$ was obtained. This material contains both Ni^{2+} and Fe^{3+}, both of which can bind to the phosphate groups of phosphopeptides. At the same time, PEI can improve its purification and enrichment performance. The $NiFe_2O_4$ metal oxide in this material is magnetic and can be rapidly separated from solution with the aid of a magnet. Loading $NiFe_2O_4$ on the GO substrate can overcome the aggregation of magnetic nanoparticles. The enrichment process of GO@PEI-$NiFe_2O_4$ for phosphopeptides is shown in Fig. 1B. Phosphorylated proteins were digested with trypsin, and the digest was mixed with the prepared magnetic composite to achieve specific recognition of phosphopeptides in the enzymatic hydrolysate. The composite was washed, and the eluate was obtained for purification and enrichment of phosphopeptides, followed by mass spectrometry analysis. GO@PEI-$NiFe_2O_4$ was prepared by a one-step method, and the purification and enrichment process for phosphopeptides was simple and rapid.

Figure 1 (A) Schematic of preparation of NiFe2O4-graphene oxide (GO) nanocomposite modified with polyethylenimine (PEI), namely GO@PEI-NiFe2O4; (B) Phosphopeptide enrichment and further analysis process by mass spectrometry (MS)

3.2 Structural characterization of GO@PEI-NiFe2O4

The morphology and elemental distribution of GO@PEI-$NiFe_2O_4$ are shown in Fig. 2. The field emission scanning electron microscope image of the substrate material GO (Fig. 2A) shows a smooth and flat surface. After modification of PEI and $NiFe_2O_4$ on the surface to form GO@PEI-$NiFe_2O_4$ composite, the surface became rough (Fig. 2B). From the partially enlarged view in Fig. 2C, it can be observed that the rough surface is composed of many fine spherical particles. Field emission transmission electron microscopy (TEM) and energy-dispersive X-ray spectroscopy (EDX) were used to analyze the GO@PEI-$NiFe_2O_4$ material (Fig. 2C), and compared with GO and GO@$NiFe_2O_4$. From the TEM images, it can be seen that the GO material surface is smooth (Fig. 2D), consistent with the SEM results. The surface of GO@$NiFe_2O_4$ is distributed with many fine spherical particles (Fig. 2E). By comparison, it is inferred that these particles are $NiFe_2O_4$. The surface morphology of the composite GO@PEI-$NiFe_2O_4$ modified with PEI (Fig. 2F) is similar to that of GO@$NiFe_2O_4$, indicating that the introduction of PEI does not significantly change the morphology of the material. The distribution of characteristic elements (C, O, N, Fe and Ni) in GO@PEI-$NiFe_2O_4$ was analyzed by EDX (Fig. 2H~2M). The results show that each element is evenly distributed in the material. The above results preliminarily confirm the successful preparation of the magnetic composite GO@PEI-$NiFe_2O_4$ with good uniformity.

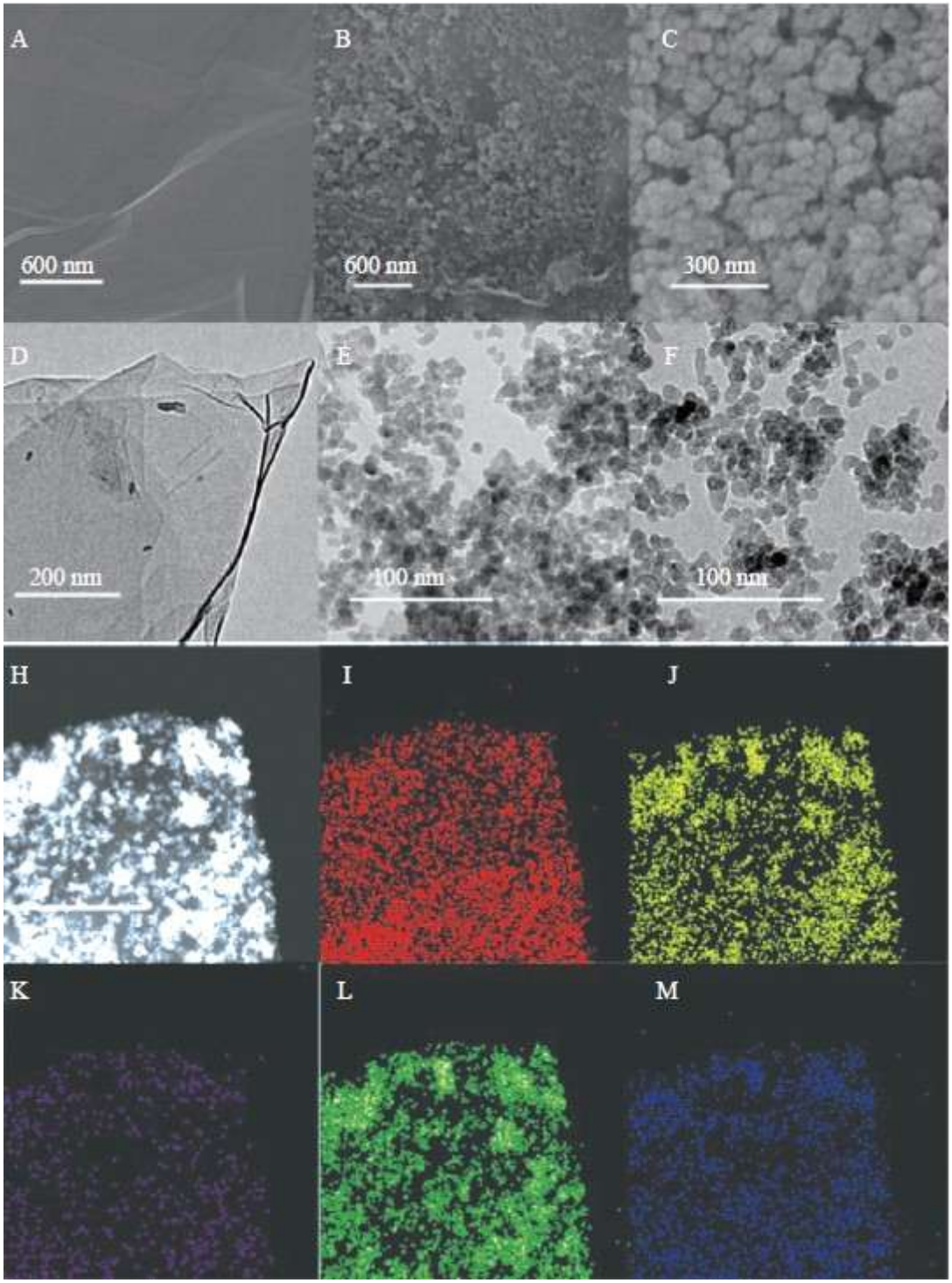

Figure 2 Scanning electron microscopy images of GO (A) and GO@PEI-NiFe2O4 (B, C), and transmission electron microscopy (TEM) images of GO (D), GO@NiFe2O4 (E) and GO@PEI-NiFe2O4 (F); TEM image of partial GO@PEI-NiFe2O4 (H) and corresponding elemental distribution of C (I), O (J), N (K), Fe (L) and Ni (M)

X-ray diffraction (XRD) was used to further analyze GO@PEI-$NiFe_2O_4$ and compare it with $NiFeO_4$ and GO@$NiFe_2O_4$. As shown in Fig. 3A, by comparing with standard XRD card data, it was found that in GO@PEI-$NiFe_2O_4$, there are diffraction peaks at 1(111), 2(220), 3(311), 4(222), 7(400), 9(422), 10(511), 12(440), 13(620), 14(533) and 18(444) (spectrum c in Fig. 3A), which can be matched to cubic spinel $NiFe_2O_4$ [26]. The

material also has three diffraction peaks at 8(011), 16(200) and 17(220), belonging to cubic Ni single substance, indicating the presence of a small amount of Ni impurity in the synthesized composite. Compared with GO@$NiFe_2O_4$, the two materials have the same types and numbers of diffraction peaks, but different peak intensities. For example, the intensity of diffraction peaks attributed to $NiFe_2O_4$ in GO@PEI-$NiFe_2O_4$ is slightly higher than that in GO@$NiFe_2O_4$, while the intensity of diffraction peaks attributed to Ni single substance is slightly lower than that in GO@$NiFe_2O_4$, indicating that the functional component $NiFe_2O_4$ has a higher content in GO@PEI-$NiFe_2O_4$. The XRD result of $NiFeO_4$ material is shown as spectrum a in Fig. 3A. The number of diffraction peaks of $NiFeO_4$ is the same as that of GO@PEI-$NiFe_2O_4$, but Ni has four more peaks (5(010), 6(002), 11(012) and 15(103)). Calculated by the software equipped with the instrument, the proportions of $NiFeO_4$ in $NiFeO_4$, GO@$NiFe_2O_4$ and GO@PEI-$NiFe_2O_4$ are 60%, 76% and 82%, respectively, indicating that the functional component $NiFe_2O_4$ has the highest proportion in GO@PEI-$NiFe_2O_4$.

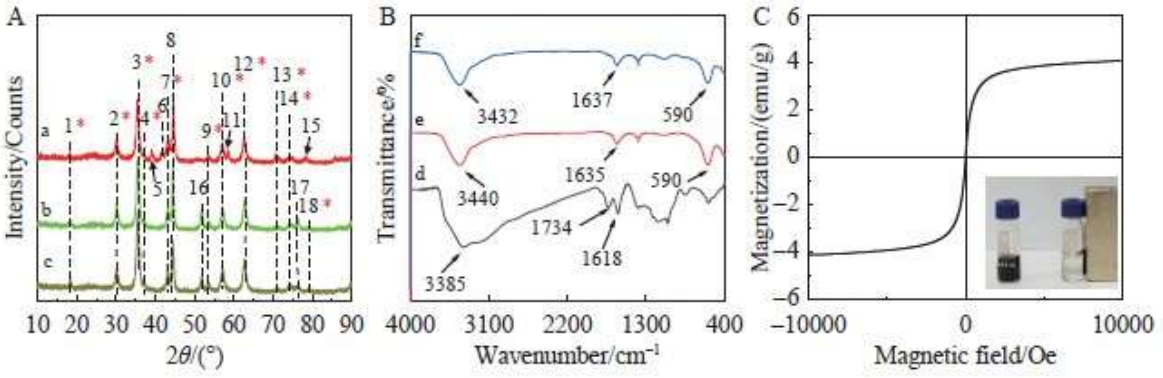

Figure 3 (A) X ray diffraction (XRD) patterns of NiFe2O4 (a), GO@NiFe2O4 (b) and GO@PEI-NiFe2O4 (c), peak information: 1(111), 2(220) , 3(311) , 4(222) , 5(010) , 6(002) , 7(400) , 8(011) , 9(422) , 10(511) , 11(012) , 12(440) , 13(620) , 14(533) , 15(103) , 16(200) , 17(220) , 18(444). The peaks marked with * represent NiFe2O4 and those with no mark stand for Ni. (B) Fourier transform infrared spectra of GO(d), GO@NiFe2O4 (e) and GO@PEI-NiFe2O4 (f). (C) Magnetic hysteresis curve of GO@PEI-NiFe2O4

The Fourier transform infrared (FTIR) spectra of the three materials are shown in Fig. 3B. In the FTIR spectrum of GO, three peaks appear at 3385, 1734 and 1618 cm^{-1}, belonging to the stretching vibrations of O-H, C=O and C=C, respectively. In the FTIR spectra of GO@$NiFe_2O_4$ and GO@PEI-$NiFe_2O_4$, a medium-intensity peak appears at 589 cm^{-1}, which can be assigned to the absorption band of $NiFe_2O_4$, corresponding to the stretching vibration of metal ions at tetrahedral sites [30-31], further verifying the spinel structure of $NiFe_2O_4$ in the material. In the spectrum of GO@PEI-$NiFe_2O_4$, the absorption band at 3432 cm^{-1} is the stretching vibration of O-H, and the absorption band at 1637 cm^{-1} can be attributed to the deformation vibration of O-H [32-33]. The FTIR spectra of GO@$NiFe_2O_4$ and GO@PEI-$NiFe_2O_4$ are similar, probably because the amount of PEI introduced is relatively small and not reflected in the infrared spectrum. From the magnetic hysteresis curve of GO@PEI-$NiFe_2O_4$ composite (Fig. 3C), it can be seen that the saturation magnetization of this magnetic material is 4.11 emu/g. The inset in Fig. 3C shows that this magnetic material can be rapidly separated from solution by a magnet.

3.3 Enrichment performance of GO@PEI-NiFe2O4 composite for phosphopeptides

β-Casein is a phosphorylated protein with many phosphorylation sites, and its digest is often used as a control to evaluate the enrichment performance of materials (detected by MALDI-TOF). When the tryptic digest of β-casein was not purified and enriched by GO@PEI-$NiFe_2O_4$ composite, no phosphopeptides could be detected by MALDI-TOF, and only non-phosphopeptide information was present in the mass spectrum (Fig. 4A), indicating that the abundance of phosphopeptides in the digest was low, and without purification and enrichment, their signals could not be detected. In addition, high-abundance non-phosphopeptides and other interfering components in the digest would suppress the mass spectrometric signals of low-abundance phosphopeptides. After the digest was purified and enriched by GO@$NiFe_2O_4$ material (without PEI modification), three phosphopeptides could be observed in the mass spectrum (Fig. 4B), and the signals of non-phosphopeptides were very weak. After treatment with GO@PEI-$NiFe_2O_4$ composite, five phosphopeptides could be observed in

DOI:

the mass spectrum (Fig. 4C), and the signals of non-phosphopeptides were further weakened, indicating that its enrichment effect for phosphopeptides was significantly better than that of the composite GO@$NiFe_2O_4$ without PEI modification. The above results show that GO@$NiFe_2O_4$ composite can bind to phosphopeptides and remove the interference of non-phosphopeptides. The introduction of PEI into GO@PEI-$NiFe_2O_4$ magnetic composite enhances its hydrophilicity and improves the enrichment performance, enabling it to enrich more phosphopeptides.

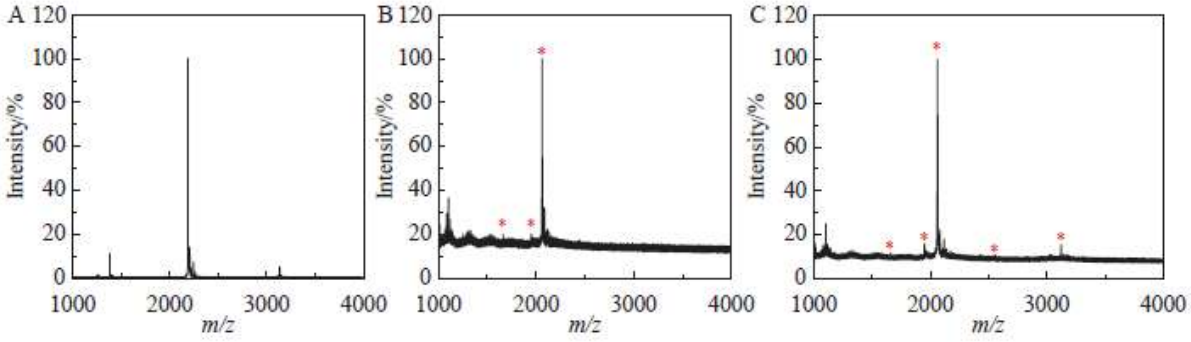

Figure 4 Mass spectra of tryptic digest for β-casein (8×10–7 mol/L) solutions: (A) Untreated; Enriched by GO@NiFe2O4 (B) and GO@PEI-NiFe2O4 (C), respectively. The peaks marked with * represent phosphopeptides

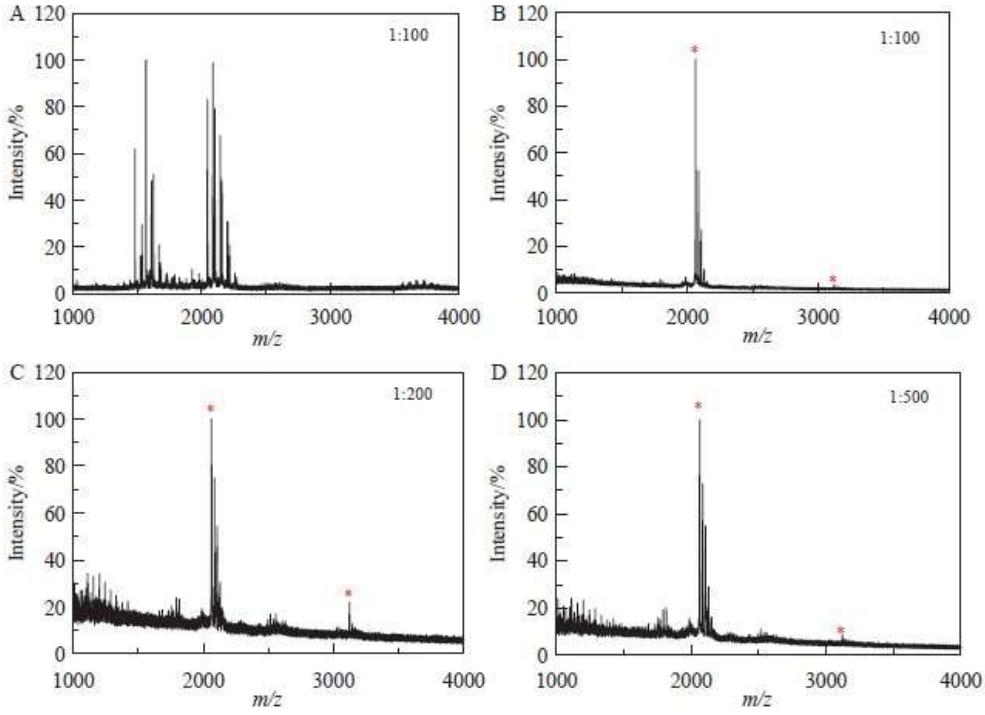

Figure 5 Mass spectra of tryptic digest mixtures for β-casein (8.00×10–8 mol/L) and BSA with different molar ratios: (A) 1∶100, untreated; (B) 1∶100, (C) 1∶200, and (D) 1∶500 enriched by GO@PEI-NiFe2O4. The peaks marked with * represent phosphopeptides

The enrichment performance of GO@PEI-$NiFe_2O_4$ magnetic composite in the presence of interfering components was further evaluated. The digest of β-casein was mixed with different concentrations of non-phosphorylated protein BSA digest (β-casein concentration fixed at 8.0×10^{-8} mol/L, molar ratios of β-casein to BSA were 1:100, 1:200 and 1:500) to increase the complexity of the system. After purification and enrichment by GO@PEI-$NiFe_2O_4$ composite, the MALDI-TOF mass spectra of the mixed digests are shown in Fig. 5. When the

mixed digest (molar ratio 1:100) was directly detected by mass spectrometry without purification and enrichment, only signals of non-phosphopeptides were present in the spectrum, and no phosphopeptides were detected (Fig. 5A). After enrichment by GO@PEI-$NiFe_2O_4$ composite, two phosphopeptides were detected (Fig. 5B). When the molar ratio of β-casein to BSA in the mixed digest was increased to 1:200 and 1:500, two phosphopeptides could still be detected in the mass spectra of the samples after purification and enrichment (Fig. 5C and 5D). Fig. 5C and 5D are results corrected by relative peak intensity. The actual peak intensities of the two phosphopeptides decreased significantly with the increase of the proportion of interfering substance BSA. This result shows that GO@PEI-$NiFe_2O_4$ has very high specific recognition ability for phosphopeptides and can effectively remove the influence of high-abundance interfering components in complex biological samples.

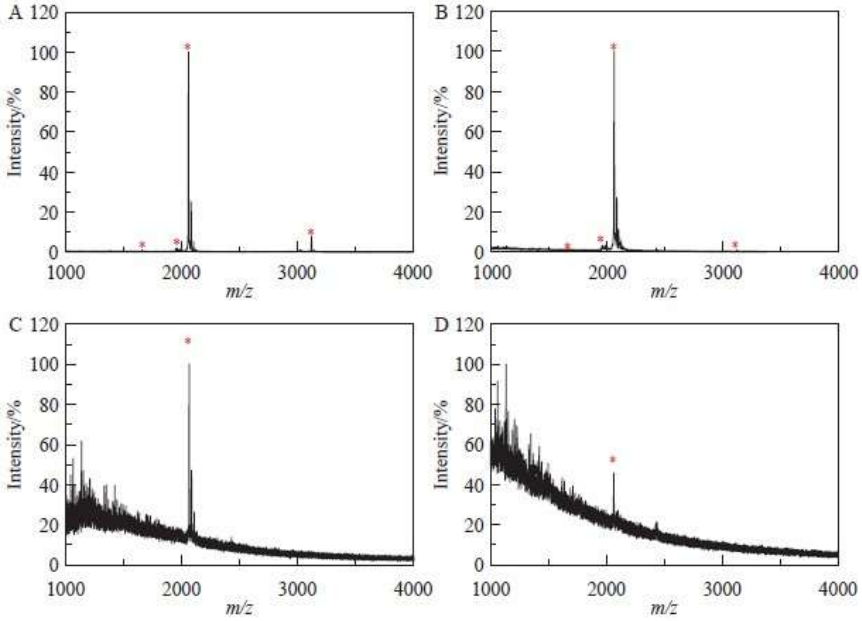

Figure 6 Mass spectra for the tryptic digests β-casein with concentrations of (A) 8.0 × 10–8 mol/L, (B) 4.0 × 10–8 mol/L, (C) 4.0 × 10–9 mol/L and (D) 4.0 × 10–10 mol/L after purification and enrichment by GO@PEI-NiFe2O4 sorbent. The peaks marked with * represent phosphopeptides

Tryptic digests of β-casein at different concentrations (8.0×10^{-8} mol/L, 4.0×10^{-8} mol/L, 4.0×10^{-9} mol/L and 4.0×10^{-10} mol/L) were purified and enriched by GO@PEI-$NiFe_2O_4$, and the mass spectra are shown in Fig. 6. When the concentration of β-casein was 8.0×10^{-8} mol/L, four phosphopeptides could be detected (Fig. 6A). When the concentration of β-casein was reduced to 4.0×10^{-8} mol/L, although the peak intensities of phosphopeptides decreased, four phosphopeptides could still be detected (Fig. 6B). When the concentration of β-casein was further reduced to 4.0×10^{-9} mol/L and 4.0×10^{-10} mol/L, the phosphopeptide at m/z 2061.0 could still be detected after purification and enrichment, but the peak intensity weakened with decreasing concentration, indicating that the prepared magnetic composite can be used for the enrichment of low-concentration phosphopeptides.

3.4 Adsorption performance of GO@PEI-NiFe2O4 for phosphopeptides

The adsorption performance of GO@PEI-$NiFe_2O_4$ for phosphopeptides was investigated. The phosphopeptide pTyr with amino acid sequence STSSDQPS[pY]SL (Mw 1380.31) was selected, and the static and dynamic adsorption processes were examined. When the amount of GO@PEI-$NiFe_2O_4$ was fixed, the adsorption curves within the concentration range of 50.0–1500 μg/mL of pTyr are shown in Fig. 7A. When the pTyr concentration was in the range of 50.0–200 μg/mL, the adsorption amount of the material increased rapidly with increasing concentration. Continuing to increase the pTyr concentration, the adsorption amount increased slowly and reached a maximum at 800 μg/mL and then tended to be stable. The adsorption capacity calculated from the adsorption curve was 36.2 μg/mg. From Fig. 7B, it can be seen that the adsorption amount of pTyr increased rapidly with the extension of adsorption time in the initial stage (0–10 min), then the growth rate slowed down

(10–20 min) and gradually reached equilibrium, indicating that this composite can rapidly adsorb phosphopeptides.

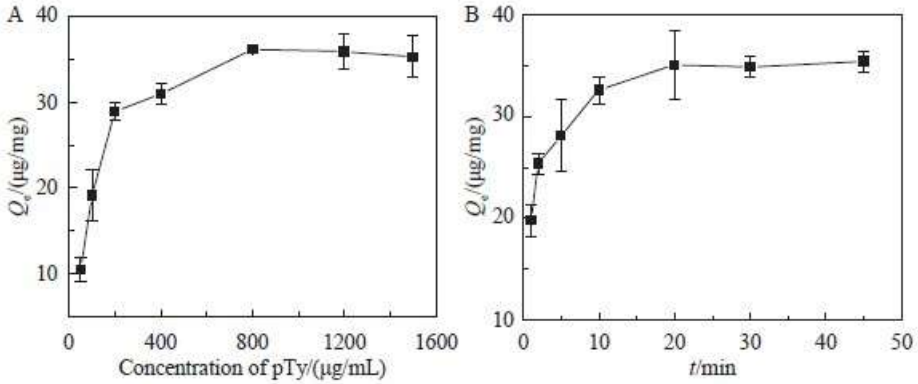

Figure 7 Adsorption curves of GO@PEI-NiFe2O4 for pTyr: (A) Adsorption isotherm curve; (B) dynamic adsorption curve

3.5 Application of GO@PEI-NiFe2O4 composite in biological samples

Tryptic digest of rat liver proteins was used as a complex biological sample to investigate the purification and enrichment performance of GO@PEI-$NiFe_2O_4$ composite for its phosphopeptides, and compared with the enrichment performance of TiO_2 and Fe^{3+}-IMAC commercial kits. After purification and enrichment, the eluates were analyzed by nano LC-MS mass spectrometry, and the obtained mass spectrometry data were searched against a spectral library. Fig. 8A shows the statistical results of the number of phosphorylation sites, phosphopeptides and proteins. After enrichment by GO@PEI-$NiFe_2O_4$ composite, a total of 1793 phosphorylation sites were detected in the eluate, corresponding to 1535 phosphopeptides and 827 phosphorylated proteins. After enrichment by TiO_2, 1805 phosphorylation sites were detected, slightly higher than that of GO@PEI-$NiFe_2O_4$, but the matched number of phosphopeptides (1515) and phosphorylated proteins (804) was lower than that of GO@PEI-$NiFe_2O_4$. This is because the proportion of multi-phosphorylated peptides enriched by TiO_2 kit (17.2%) was higher than that of GO@PEI-$NiFe_2O_4$ (15.8%). After enrichment by Fe^{3+}-IMAC kit, a total of 925 phosphorylation sites, 818 phosphopeptides and 512 phosphorylated proteins were detected, which were significantly lower than the enrichment performance of GO@PEI-$NiFe_2O_4$ and TiO_2.

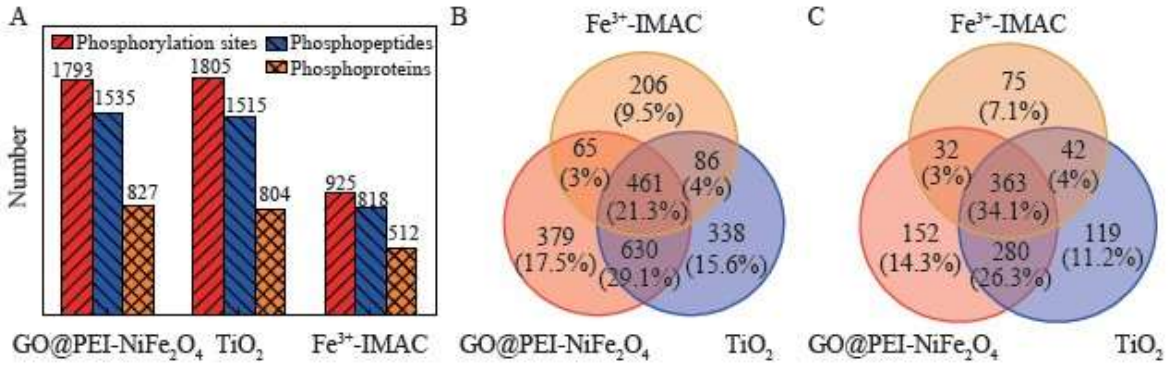

Figure 8 The number of phosphorylation sites, phosphopeptides and phosphoproteins of tryptic digest of rat liver protein enriched by GO@PEI-NiFe2O4, TiO2 kit and Fe3+-IMAC, respectively (A); the Venn diagrams of the corresponding phosphopeptieds (B) and phosphoproteins (C)

Table 1. Compositional and Structural Properties of GO-Based Composites

Material	Preparation Method	Key Structural Features	$NiFe_2O_4$ Content (%)	Saturation Magnetization (emu/g)	Surface Morphology
$NiFeO_4$	Solvothermal (200°C, 24 h)	Spinel $NiFe_2O_4$ nanoparticles	60	Not reported	Agglomerated particles
GO@$NiFe_2O_4$	Solvothermal (no PEI)	$NiFe_2O_4$ nanoparticles on GO sheets	76	Not reported	Fine spherical particles uniformly distributed on GO
GO@PEI-$NiFe_2O_4$	One-step solvothermal (GO + PEI + Ni/Fe salts)	PEI-modified; $NiFe_2O_4$ on GO; rough surface	82	4.11	Rough surface composed of fine spherical particles; elements (C,O,N,Fe,Ni) evenly distributed

Table 2. Phosphopeptide Enrichment Performance from β-Casein Tryptic Digest (MALDI-TOF)

Material / Condition	Non-phosphopeptide Interference	Number of Phosphopeptides Detected	Phosphopeptides Identified (m/z)	Notes
No enrichment (control)	Severe	0	—	Only non-phosphopeptide signals observed
GO@$NiFe_2O_4$ (without PEI)	Weak	3	Not specified	Baseline enrichment capability
GO@PEI-$NiFe_2O_4$	Very weak (further suppressed)	5	2061.0 and others	PEI enhanced hydrophilicity → improved selectivity
GO@PEI-$NiFe_2O_4$ (β-casein 8.0×10^{-8} mol/L)	Low	4	2061.0 etc.	Clear phosphopeptide signals
GO@PEI-$NiFe_2O_4$ (β-casein 4.0×10^{-8} mol/L)	Low	4	2061.0 etc.	Peak intensities decreased with concentration
GO@PEI-$NiFe_2O_4$ (β-casein 4.0×10^{-9} mol/L)	Low	1	2061.0	Lowest concentration tested; single peptide still detected
GO@PEI-$NiFe_2O_4$ (β-casein 4.0×10^{-10} mol/L)	Low	1	2061.0	Signal further weakened but detectable

Table 3. Anti-Interference Capability in Complex Matrices (β-Casein : BSA Mixtures)

Molar Ratio (β-casein : BSA)	Enrichment Material	Phosphopeptides Detected	Non-phosphopeptide Suppression	Key Finding
1 : 100	None (direct MS)	0	Poor	No phosphopeptides detected
1 : 100	GO@PEI-$NiFe_2O_4$	2	Effective	Enrichment enabled detection
1 : 200	GO@PEI-$NiFe_2O_4$	2	Effective	Performance maintained at 200-fold excess BSA
1 : 500	GO@PEI-	2	Effective	Successful enrichment even

	$NiFe_2O_4$			at 500-fold excess BSA

Table 4. Adsorption Capacity, Kinetics, and Biological Sample Benchmarking

Parameter / Material	GO@PEI-$NiFe_2O_4$	TiO_2 Kit	Fe^{3+}-IMAC Kit	Notes
Model phosphopeptide	pTyr (STSSDQPS[pY]SL)	—	—	—
Max. adsorption capacity (static)	36.2 μg/mg	—	—	Saturation at pTyr 800 μg/mL
Equilibrium time (dynamic)	10–20 min	—	—	Rapid adsorption; >90% capacity within 10 min
Rat liver digest: Phosphorylation sites	1793	1805	925	TiO_2 slightly higher in sites; GO@PEI-$NiFe_2O_4$ comparable
Rat liver digest: Phosphopeptides	1535	1515	818	GO@PEI-$NiFe_2O_4$ identified the most phosphopeptides
Rat liver digest: Phosphorylated proteins	827	804	512	GO@PEI-$NiFe_2O_4$ identified the most proteins
Multi-phosphorylated peptides (%)	15.8%	17.2%	Not reported	TiO_2 favors multi-phosphorylated species
Common phosphopeptides (vs. TiO_2)	60.4% overlap	60.4% overlap	—	Similar metal-oxide mechanism; complementary
Common phosphopeptides (vs. Fe^{3+}-IMAC)	24.3%	—	24.3%	Different recognition mechanism (Fe^{3+} vs. $NiFe_2O_4$)

Table 5. Mechanistic Contribution of Each Component to Overall Performance

Component	Primary Role	Performance Contribution	Evidence from Paper
$NiFe_2O_4$ (spinel)	Dual-metal (Ni^{2+}/Fe^{3+}) Lewis acid sites	Bidentate/tridentate coordination with phosphate groups; higher site density (82% content)	XRD, FTIR (589 cm^{-1}), enrichment of 5 phosphopeptides
PEI (Mw ~70 000)	Hydrophilicity enhancer	Creates hydration layer; suppresses non-specific hydrophobic binding; improves dispersion	MALDI-TOF: 5 vs. 3 peptides (with/without PEI); high BSA tolerance
GO nanosheets	Structural scaffold	Prevents magnetic aggregation; increases surface area; provides additional –OH/–COOH sites	TEM/SEM: uniform particle distribution; fast magnetic separation (4.11 emu/g)
Magnetic responsen	Rapid separation	Enables magnet-assisted isolation within seconds	Photo inset (Fig. 3C): instant separation

Venn diagrams were used to compare and analyze the number of phosphopeptides and proteins detected after enrichment by the three materials (Fig. 8B and 8C). The results show that the three materials could commonly enrich about 21.3% of phosphopeptides, corresponding to 34.1% of proteins, indicating significant differences in their properties. From Fig. 8B, it can be seen that 50.4% of phosphopeptides enriched by GO@PEI-$NiFe_2O_4$ composite and TiO_2 kit were the same, corresponding to 60.4% of phosphorylated proteins. However, only 24.3% of phosphopeptides were simultaneously enriched by GO@PEI-$NiFe_2O_4$ and Fe^{3+}-IMAC kit, corresponding to 37.1% of phosphorylated proteins. Because the functional groups for recognizing phosphopeptides in GO@PEI-$NiFe_2O_4$ and TiO_2 are both metal oxides, more identical phosphopeptides were enriched. Fe^{3+}-IMAC plays a key role in the enrichment process through Fe^{3+}, which is different from GO@PEI-$NiFe_2O_4$, so fewer identical phosphopeptides were enriched. Although the percentage of identical phosphopeptides enriched by GO@PEI-$NiFe_2O_4$ and TiO_2 was relatively high, there were still more than 440 and 420 peptides enriched only by

each of the two materials, respectively, indicating that their enrichment mechanisms are not completely the same, and these two materials can complement each other to a certain extent.

3.6 In-depth mechanistic insights into the enhanced enrichment performance

The superior phosphopeptide enrichment capability of GO@PEI-$NiFe_2O_4$ compared with unmodified $NiFe_2O_4$, GO@$NiFe_2O_4$, and commercial kits stems from a synergistic combination of multiple physicochemical and structural factors. These factors collectively address the intrinsic limitations of conventional metal oxide affinity materials and significantly improve selectivity, adsorption capacity, kinetics, and anti-interference ability in complex matrices.

3.6.1 Multivalent metal coordination and synergistic binding effects

The surface of GO@PEI-$NiFe_2O_4$ presents abundant Ni^{2+} and Fe^{3+} ions derived from the spinel-structured $NiFe_2O_4$ nanocrystals. Both metal ions act as strong Lewis acid sites that can form bidentate or tridentate coordination complexes with the phosphate groups of phosphopeptides [15,16,25,26]. Unlike single-metal oxides (e.g., TiO_2 or Fe_3O_4), the simultaneous presence of Ni^{2+} and Fe^{3+} creates a dual-coordination environment that increases the probability of multidentate binding to a single phosphopeptide, thereby strengthening the overall interaction and enhancing selectivity, especially for mono-phosphorylated peptides. The XRD analysis confirmed a high $NiFe_2O_4$ content (82 wt%) in the composite, which ensures a dense distribution of these active sites. Furthermore, the magnetic hysteresis loop showed a saturation magnetization of 4.11 emu/g, which is sufficient for rapid magnetic separation without causing irreversible aggregation, thus maintaining the accessibility of the metal sites during enrichment.

3.6.2 Hydrophilicity enhancement via PEI modification

A major drawback of most MOAC materials is their low intrinsic hydrophilicity, which leads to non-specific adsorption of hydrophobic non-phosphopeptides and reduces enrichment specificity. In this work, polyethyleneimine (PEI, Mw ~70 000) was covalently anchored onto the composite surface. PEI is a water-soluble polycationic polymer rich in primary, secondary, and tertiary amines. These amine groups readily form hydrogen bonds with water molecules, creating a robust hydration layer that dramatically increases the surface hydrophilicity of the material. As a result, the hydrophilic-hydrophobic balance is shifted in favor of phosphopeptide retention: hydrophilic phosphopeptides are preferentially attracted to the hydrated surface, while hydrophobic non-phosphopeptides are repelled. Comparative MALDI-TOF experiments (Fig. 4) directly demonstrated this effect—GO@PEI-$NiFe_2O_4$ enriched five phosphopeptides from β-casein digest, whereas GO@$NiFe_2O_4$ (without PEI) only yielded three, and the background signals from non-phosphopeptides were markedly lower after PEI modification. The enhanced hydrophilicity also improves the dispersion stability of the composite in polar loading/washing solvents (e.g., 50 % ACN/5 % FA), preventing agglomeration and ensuring maximum exposure of the Ni^{2+}/Fe^{3+} sites.

3.6.3 Dispersion promotion by graphene oxide support

The two-dimensional GO nanosheets serve as an ideal scaffold for growing $NiFe_2O_4$ nanoparticles. TEM images (Fig. 2E,F) revealed that the nanoparticles are uniformly distributed on the GO surface without significant aggregation. This spatial isolation is crucial because bare $NiFe_2O_4$ nanoparticles tend to form large clusters due to their high magnetic dipole interactions, which severely reduce the available surface area. GO not only physically separates the nanoparticles but also provides additional oxygen-containing functional groups (-OH, -COOH, epoxides) that contribute weak hydrophilic interactions and may participate in hydrogen bonding with phosphopeptides. The high aspect ratio and flexibility of GO further increase the hydrodynamic radius of the composite, facilitating rapid magnetic sedimentation while minimizing diffusion limitations during peptide binding.

3.6.4 Synergistic electrostatic and hydrophilic interactions

Under the acidic loading conditions (solvent A: 50 % ACN, 5 % FA, pH ≈ 2–3), phosphopeptides carry multiple

negative charges on their phosphate groups, while the PEI amine groups become partially protonated, acquiring positive charges. This creates a favorable electrostatic attraction that complements the Lewis acid-base coordination. Non-phosphopeptides, lacking such strongly acidic groups, remain mostly neutral or weakly negatively charged and therefore experience little electrostatic pull. The combined effect of electrostatic attraction, multivalent metal coordination, and hydrophilic exclusion of hydrophobic competitors endows GO@PEI-$NiFe_2O_4$ with exceptional specificity, as evidenced by the successful enrichment from highly complex rat liver digests (Fig. 8) where 1535 phosphopeptides were identified—outperforming both TiO_2 and Fe^{3+}-IMAC kits.

3.6.5 Fast adsorption kinetics and high capacity

The dynamic adsorption curve (Fig. 7B) shows that equilibrium is reached within 20 min, which is attributed to the high dispersibility of the composite and the short diffusion pathways on the thin GO sheets. The static adsorption capacity of 36.2 μg/mg for pTyr is among the highest reported for magnetic MOAC materials. This large capacity originates from the high loading of $NiFe_2O_4$ (82 % by XRD) and the fact that PEI, despite its low mass fraction, creates a loosely packed “polymer brush” layer that does not block but rather promotes peptide access to the underlying metal sites.

3.6.6 Anti-interference capability in complex matrices

The material’s ability to selectively enrich phosphopeptides in the presence of a 500-fold excess of BSA digest (Fig. 5) is a direct consequence of the above mechanisms. The hydrated PEI layer effectively suppresses the adsorption of high-abundance non-phosphoproteins, while the strong multidentate coordination ensures that low-abundance phosphopeptides are still captured. This performance is critical for real-world phosphoproteomics, where dynamic ranges often exceed four orders of magnitude.

In summary, the performance enhancement of GO@PEI-$NiFe_2O_4$ is not driven by a single factor but by a rational integration of (i) high-density dual-metal coordination sites, (ii) hydrophilicity-driven suppression of non-specific binding via PEI, (iii) dispersion and stabilization by GO, and (iv) favorable electrostatic interactions under acidic conditions. This multi-pronged strategy successfully overcomes the traditional bottlenecks of MOAC materials and provides a robust platform for large-scale phosphopeptide enrichment.

4 Conclusion

A magnetic enrichment material GO@PEI-$NiFe_2O_4$ with specific recognition ability for phosphopeptides was successfully prepared by loading spinel-structured $NiFe_2O_4$ on GO surface via a one-step method and modifying it with hydrophilic PEI. This material is easy to prepare, has a high adsorption capacity for phosphopeptides, and the adsorption is rapid. During the enrichment process, it can effectively remove the interference of non-phosphorylated components. This material has good purification and enrichment ability for phosphopeptides, and its enrichment effect is significantly better than that of commercial kits such as Fe^{3+}-IMAC, showing good application potential in phosphoproteomics research. This study provides a new strategy for the preparation of phosphopeptide enrichment materials.

References

[1] HIEU H, ARMINJA A K. Trends Biochem. Sci., 2023, 48(8): 713-725.
[2] HUNTER T. Cell, 2000, 100(1): 113-127.
[3] COHEN P. Trends Biochem. Sci., 2000, 25(12): 596-601.
[4] ZAGORAC I, FERNANDEZ-GAITERO S, PENNING R, POST H, BUENO M J, MOURON S, MANSO L, MORENTE M M, ALONSO S, SERRA V, MUNOZ J, GOMEZ-LOPEZ G, FRANCISCO LOPEZ-ACOSTA J, JIMENEZ-RENARD V, GRIS-OLIVER A, AL-SHAHROUR F, PINEIRO-YANEZ E, LUIS MONTOYA-SUAREZ J, APALA J V, MORENO-TORRES A, COLOMER R, DOPAZO A, HECK A J R, ALTELAAR M, QUINTELA-FANDINO M. Nat. Commun., 2018, 9 (1): 3501.

[5] BATISTA T M, JAYAVELU A K, ALBRECHTSEN N J W, IOVINO S, LEBASTCHI J, PAN H, DREYFUSS J M, KROOK A, ZIERATH J R, MANN M, KAHN C R. Cell Metab., 2020, 32(5): 844-859.
[6] LEE K M, GILTNANE J M, BALKO J M, SCHWARZ L J, GUERRERO-ZOTANO A L, HUTCHINSON K E, NIXON M J, ESTRADA M V, SANCHEZ V, SANDERS M E, LEE T, GOMEZ H, LLUCH A, PEREZ-FIDALGO A, WOLF M M, AND REJEVA G, RATHMELL J C, FESIK S W, ARTEAGA C L. Cell Metab., 2017, 26(4): 633-647.
[7] ANWAR T, ARELLANO-GARCIA C, ROPA J, CHEN Y C, KIM H S, YOON E, GRIGSBY S, BASRUR V, NESVIZHSKII A I, MUNTEAN A, GONZALEZ M E, KIDWELL K M, NIKOLOVSKA-COLESKA Z, KLEER C G. Nat. Commun., 2018, 9(1):
[8] BECARES N, GAGE M C, VOISIN M, SHRESTHA E, MARTIN-GUTIERREZ L, LIANG N, LOUIE R, POURCET B, PELLO O M, LUONG T V, GONI S, PICHARDO-ALMARZA C, ROBERG-LARSEN H, DIAZ-ZUCCARINI V, STEFFENSEN K R, O'BRIEN A, GARABEDIAN M J, ROMBOUTS K, TREUTER E, PINEDA-TORRA I. Cell Rep., 2019, 26(4): 984-995.
[9] GAO W, ZHANG F, ZHANG S, LI J Y, LIAN H Z. Sep. Purif. Technol., 2023, 305: 122426.
[10] LI X S, YUAN B F, FENG Y Q. TrAC, Trends Anal. Chem., 2016, 78: 70-83.
[11] DOMON B, AEBERSOLD R. Science, 2006, 312(5771): 212-217.
[12] YU L Z, HE J, YAN S, LIU Y C, LAN F, WU Y. ACS Sustainable Chem. Eng., 2022, 10(7): 2094-2508.
[13] LI X W, ZHANG N, TANG R Z, LYU J W, LIU Z, MA S J, OU J J, YE M L. Nanoscale, 2021, 13(5): 2923-2930.
[14] LI J Y, ZHANG S, GAO W, HUA Y, LIAN H Z. ACS Sustainable Chem. Eng., 2020, 8(44): 16422-16429.
[15] YAN S, LUO B, YU L Z, LAN F, WU Y. ACS Sustainable Chem. Eng., 2022, 10(43): 14220-14229.
[16] ZHANG S, LI J Y, GAO W, QIAO J Q, LIAN H Z. ACS Appl. Mater. Interfaces, 2023, 15(13): 16505-16514.
[17] ZHANG L W, WANG Y, ZHANG W J, HSU Y I, ASOH T A, QI B Y, UYAMA H. ACS Biomater. Sci. Eng., 2022, 8(6): 2676-2683.
[18] WANG B C, WU H M, YAN Y H, TANG K Q, DING C F. Rapid Commun. Mass Spectrom., 2020, 34(20): e8881.
[19] JIANG D D, QI R X, LYU S Q, WANG W, LIU J H, JIA Q. Chem. Res. Chin. Univ., 2023, 39(2): 253-259.
[20] LI L P, CHEN S, XU L N, BAI Y, NIE Z X, LIU H W, QI L M. J. Mater. Chem. B, 2014, 2(9): 1121-1124.
[21] JIANG D D, LV S Q, QI R X, LIU J H, DUAN L M. J. Chromatogr. A, 2022, 1678: 463374.
[22] MEISENBICHLER C, RAUCH J S, GUZEL Y, WERNIG E M, SCHEMETH D, TRIBUS M, TESSADRI R, RAINER M. Anal. Methods, 2016, 8(15): 3061-3068.
[23] WANG M Y, DENG C H, LI Y, ZHANG X M. ACS Appl. Mater. Interfaces, 2014, 6(14): 11775-11782.
[24] HE Y T, ZHENG Q, HUANG H, JI Y, LIN Z A. Anal. Chim. Acta, 2022, 1198: 339552.
[25] ZHONG H Y, XIAO X, ZHENG S, ZHANG W Y, DING M J, JIANG H Y, HUANG L L, KANG J. Nat. Commun., 2013, 4(1): 1656.
[26] LI J Y, CAO Z M, HUA Y, WEI G, YU X Z, SHANG W B, LIAN H Z. Anal. Chem., 2020, 92(1): 1058-1067.
[27] LASHMAWI I S, ISMAIL A M. Polym. Bull., 2023, 80(3): 2329-2348.
[28] EKRI L Z, DARYA-LAAL A R. Polycyclic Aromatic Compd., 2020, 40(5): 1539-1556.
[29] HANG K N, HAO Y, HU D H, DENG S M, JIN Y H, WANG X F, LIU H L, LIU Y, XIE M X. J. Chromatogr. A, 2021, 1659: 462648.
[30] ANG S X, MAIMAITI H L D, XU B, GUO Y, ZHAI P S, ZHANG H Z. J. Phys. Chem. C, 2019, 123(51): 31119-31129.
[31] GEBRESLASSIE G, BHARALI P, CHANDRA U, SERGAWIE A, BORUAH P K, DAS M R, ALEMAYEHU E. J. Photochem. Photobiol., A, 2019, 382: 111960.
[32] ORTIZ-BUSTOS J, DEL PULGAR H P, PEREZ Y, DEL HIERRO I. Dalton Trans., 2023, 52(30): 10423-10436.
[33] XIA Y J, ZHAO F, CHENG Z G, LI Z Z, XU B C. Ceram. Int., 2022, 48(21): 32226-32235.